Journal of Structural Geology 32 (2010) 306–320

Contents lists available at ScienceDirect

Journal of Structural Geology

journal homepage: www.elsevier.com/locate/jsg

Emplacement and deformation of the Fomopéa pluton: Implication for the Pan-African history of Western Cameroon

T. Njanko [a,b], A. Nédélec [b,*], M. Kwékam [a], R. Siqueira [b], L. Esteban [c,d]

[a] LGE, Department of Earth Sciences, University of Dschang, B.P. 67 Dschang, Cameroon
[b] UMR5563-LMTG-OMP, University of Toulouse-CNRS-IRD, 14 Avenue Edouard-Belin, 31400 Toulouse, France
[c] Geological Survey of Canada-Pacific, 9860 West Saanich Road, Sidney, BC V8L 4B2, Canada
[d] CSIRO, ARRC, Petroleum Resources, 26 Dick Perry Avenue, Kensington, Perth, WA 6151, Australia

ARTICLE INFO

Article history:
Received 19 August 2008
Received in revised form
10 December 2009
Accepted 24 December 2009
Available online 6 January 2010

Keywords:
AMS
Cameroon
Granite
Pan-African
Shear zone

ABSTRACT

The Fomopéa pluton (622–613 Ma) is located in the western part of the Pan-African belt in Cameroon. It comprises of 3 units: biotite-hornblende granitoids (BHG), biotite monzogranites (BmG) and edenite syenogranites (EsG). The BHG unit displays magnetic fabrics characterized by foliations gently dipping towards the ESE and ENE-trending lineations (D1 event). Microstructures are magmatic to submagmatic. In discrete N–S deformation bands (D2), lineations are rotated towards the North and microstructures indicate solid-state deformation at mid- to low-T conditions, with kinematic indicators pointing to a sinistral motion. The second unit, BmG, displays lineation trajectories suggesting emplacement during the D2 event. The EsG unit displays fabrics consistent with a later emplacement, with no superposed deformation. The last event (D3) corresponds to a dextral shear zone, that runs along the southeastern border of the Fomopéa pluton. It was responsible for protomylonitic deformation of the granitic rocks in greenschist facies conditions, whereas the core of the shear zone registered higher temperatures and strain. This shear zone induced a rejuvenation of the Rb/Sr isotopic system in the pluton at ca 572 Ma. It belongs to the Central Cameroon shear zone system, regarded as the prolongation of the dextral Patos shear zone system in Brazil.

1. Introduction

Numerous studies have underlined the interest of granitoids as crustal scale deformation markers (e.g. Gapais, 1989; Solar et al., 1998; Nascimento et al., 2004; Sadeghian et al., 2005; Archanjo et al., 2008, among many others). According to Hutton (1997) and Brown and Solar (1998), spatial and temporal relationships between granite and regional tectonic structures suggest granite emplacement during contraction rather than during extension in many convergent orogenic belts. Granites are almost invariably linked to orogenic environments and the close correlation established between shear zone systems, transpressive convergent zones and regions of melt transfer and granite emplacement are well documented (D'Lemos et al., 1992; Ingram and Hutton, 1994; Leblanc et al., 1996; Brown and Solar, 1998). Granite emplacement and deformation during regional tectonic events is a challenging study, because granitic rocks do not always develop mesoscopic scale deformation fabrics. However, according to Simpson (1985), Paterson et al. (1989) and Bouchez et al. (1992), microstructural studies of granites can help to identify magmatic or solid-state deformation fabrics.

The Pan-African Belt of Central Africa (PBCA) is connected with the Neoproterozoic Brasiliano Fold Belt (Brito Neves et al., 2002; Cordani et al., 2003) as shown in Fig. 1a from Caby et al. (1991). However, it is less well known. In Cameroon, the Pan-African tectonic evolution is characterized by large scale shear zones, such as the Adamaoua shear zone (ASZ) and the Tcholliré-Banyo fault (TBF), that have transposed early structures (Fig. 1b). Regarding the evolution of the Pan-African belt in central and south Cameroon, Ngako et al. (2003) proposed a model related to major events of transpression and transtension during shear movements. Granite plutons spatially associated with shear zones are large composite intrusions generally made up of more than two rock types. In the central domain of the PBCA, detailed petrology of some plutons is provided: e.g. the Ngondo plutonic complex, the West Tibati plutons, the two-mica granites from the Nkambé area (Fig. 2b), respectively studied by Tagné-Kamga (2003); Njanko et al. (2006) and Tetsopgang et al. (2006). Other studies are only available in unpublished theses. Moreover, in these works, structural aspects are generally missing due to the lack of appropriate methods.

* Corresponding author. Fax: +33 5 61 33 25 60.
E-mail address: nedelec@lmtg.obs-mip.fr (A. Nédélec).

0191-8141/$ – see front matter © 2010 Elsevier Ltd. All rights reserved.
doi:10.1016/j.jsg.2009.12.007

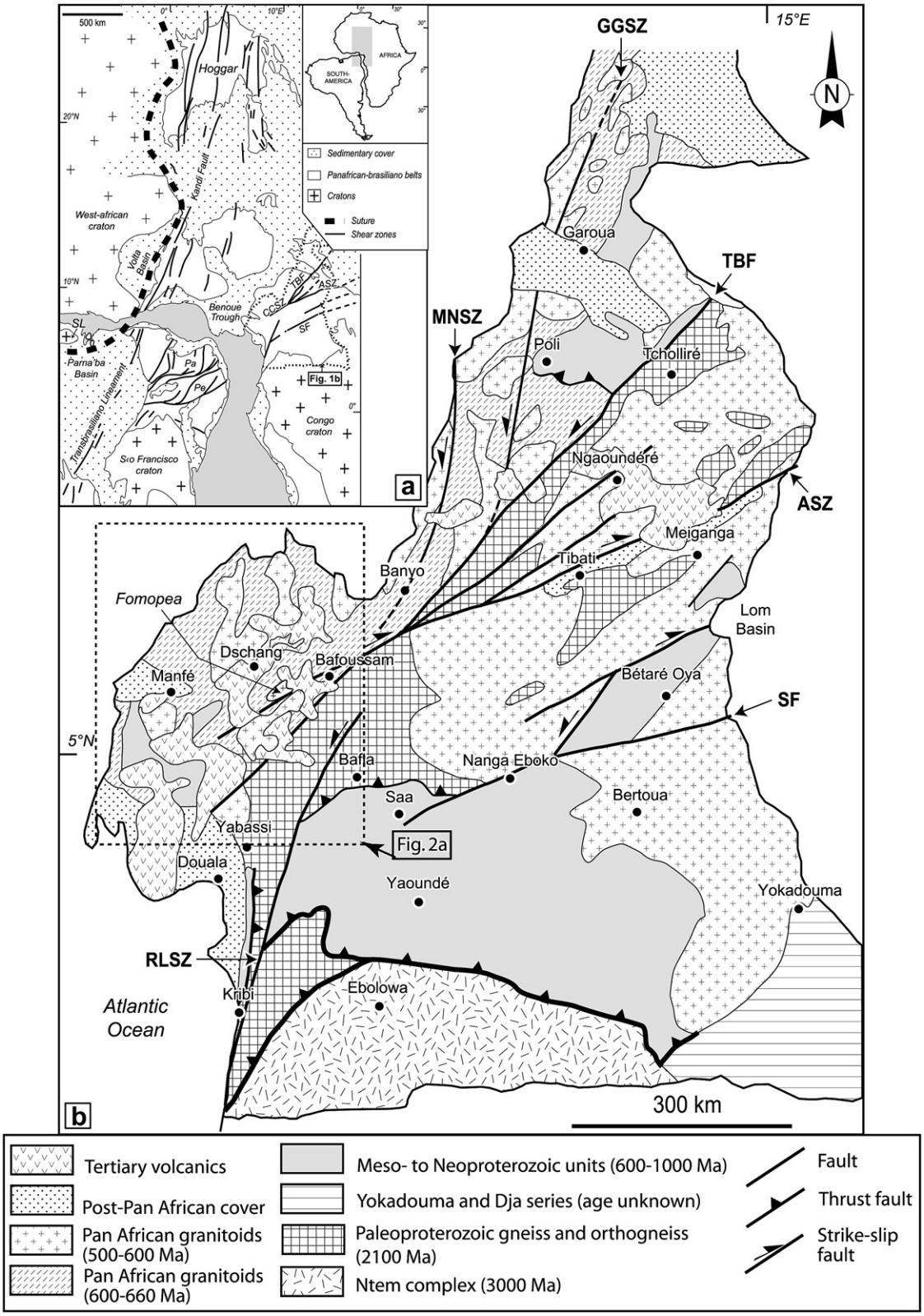

Fig. 1. (a) Pre-drift reconstruction. (b) Geological map of Cameroon showing the major lithotectonic domains (after Toteu et al., 2001, and Ngako et al., 2008). ASZ: Adamaoua shear zone; CCSZ: Central Cameroon shear zone; GCSZ: Godé-Gormaya shear zone; MNSZ: Mayo Nolti shear zone; Pa: Patos shear zone; Pe: Pernambuc shear zone; RLSZ: Rocher du Loup shear zone; SF: Sanaga fault; TBF: Tcholliré-Banyo fault.

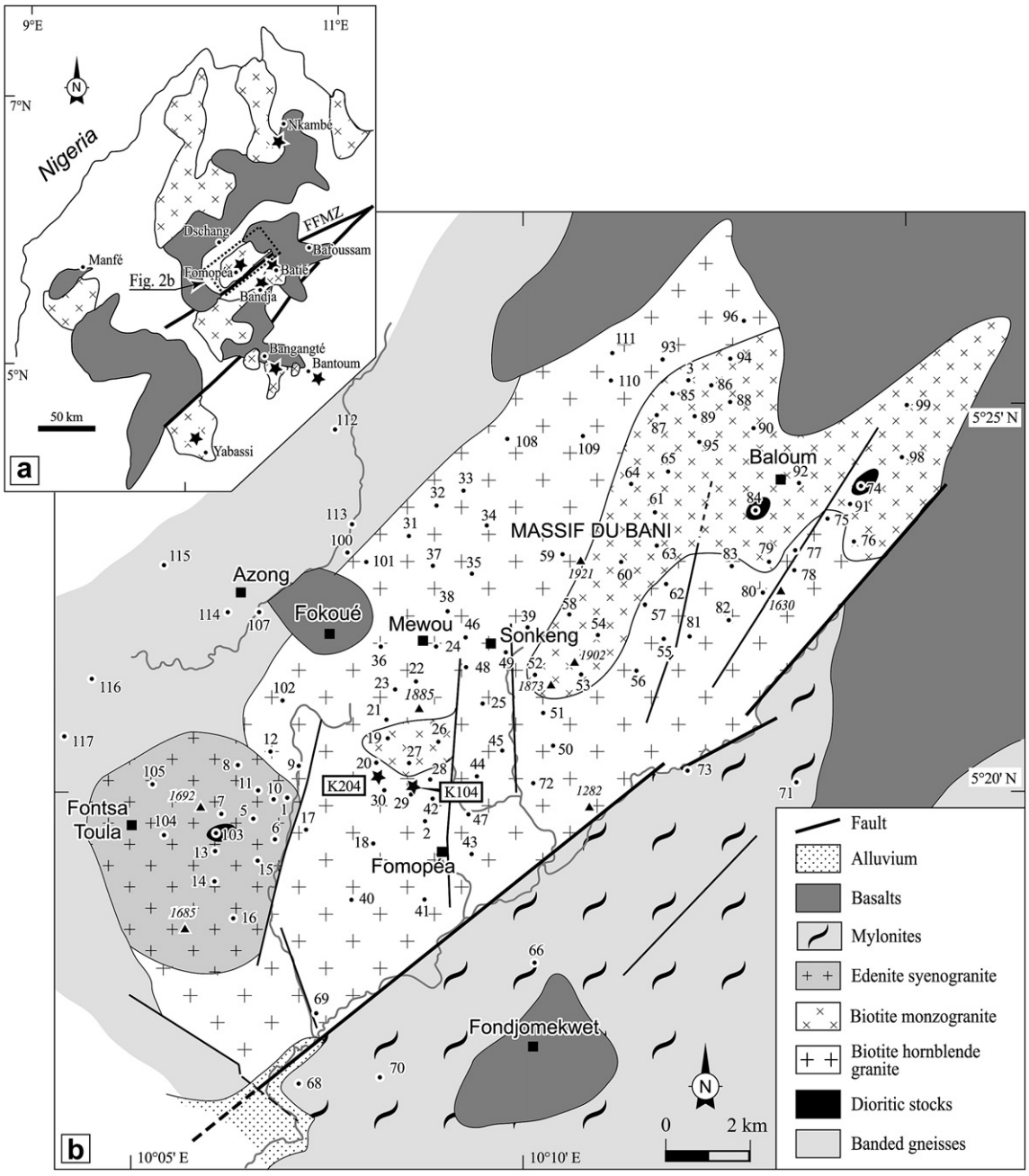

Fig. 2. (a) Geological sketch map of central lithotectonic domain (showing the previously studied plutons : stars) with available geochronological data; FFMZ = Fotouni-Fondjomekwet mylonitic zone. (b) Geological sketch map of Fomopéa granitic pluton showing the sampled stations and locations of dated samples (stars).

The purpose of this paper is to present a case in which structures and microstructures are used to reconstruct the kinematics of emplacement of the Pan-African Fomopéa pluton and its sub-solidus deformation history, using combined magnetic fabrics and microscopic observations. Up to now, in the PBCA of Cameroon, only Kankeu and Greiling (2006) carried out such a work on a small part of the Neoproterozoic basement of Eastern Cameroon. The present study focuses on Fomopéa pluton in West Cameroon, because of already available petrological and geochronological data (Kwékam, 2005; Kwékam et al., 2009), in addition to its proximity and accessibility near Dschang city. The paper starts by presenting the magnetic susceptibility with the magnetic mineralogy of the different rock types of the pluton; then, the anisotropy of magnetic susceptibility (AMS) data, providing magnetic foliations and lineations, are discussed with respect to the microstructures, i.e. magmatic or solid-state fabrics. The new structural data reveal a multi-phase deformation, enlightening the Pan-African history of West Cameroon, that has remained poorly studied so far by comparison with southern and northern Cameroon.

2. Regional geological setting

2.1. The Pan-African belt in Cameroon

Based on geochronological (Rb–Sr) works, Lasserre (1967a,b) proposed that the Precambrian basement rocks in Cameroon (Fig. 1b) were divided into two domains: the Archaean Ntem Complex and the Pan-African orogenic belt or "mobile zone". The

term "mobile zone", according to Anhaeusser et al. (1969), is applied to Precambrian metamorphic belts, characterized by medium- to high-grade metamorphism, polycyclic deformation, possible reworking of older crust and generation of new granitic magmas. The Pan-African mobile zone in Cameroon is also known as Pan-African North Equatorial Fold Belt (Nzenti et al., 1988) or Pan-African Belt of Central Africa (PBCA) (Penaye et al., 1993; Toteu et al., 2001) that will be preferentially used in this study.

The PBCA in Cameroon (Fig. 1b) used to be divided into three main lithotectonic units namely; (a) a Paleoproterozoic basement predominantly composed of heterogeneous migmatitic gneisses (Penaye et al., 1989); (b) Meso- to Neoproterozoic volcano-sedimentary basins that were deformed and metamorphosed into schists and high-grade gneisses (Nzenti et al., 1988), and (c) Pan-African granitoids that are often made of syntectonic granitoids of high-K calc-alkaline affinities (e.g. Njanko et al., 2006). Actually, Pan-African granitoids were emplaced from the early stage of the deformation (orthogneisses) to the late uplift stages of the orogen (post-tectonic sub-circular massifs), cross-cutting the two former units (Toteu et al., 2001). Several Pan-African granitoid intrusions were emplaced in spatial relation with the CCSZ (Central Cameroon Shear zone: Fig. 1a) or with the regional N30°E fault, recently reactivated as the Cameroon volcanic line. This is the case of the Fomopéa pluton.

2.2. Geology and geochronology of Fomopéa area

On the reconnaissance geological map of Dumort (1968), the Fomopéa granitic pluton is recognized with a southeastern faulted border. The northern part of the pluton is hidden by tertiary basalts. According to Kwékam (2005) and Kwékam et al. (2009), the Fomopéa granitic pluton comprises three petrographic units: (i) biotite–hornblende granitoids (BHG), including diorites, quartz-monzodiorites, quartz-monzonites, granodiorites and monzogranites, (ii) biotite monzogranites (BmG) and (iii) edenite syenogranites (EsG). BHG are medium- to coarse-grained with biotite, hornblende, plagioclase, K-feldspar and quartz as main minerals. Common accessory phase minerals are magnetite, zircon, apatite, titanite and allanite. Sometimes, magmatic epidote surrounds an allanite core. This magmatic accessory mineral is indicative of deep emplacement and/or a high O_2 fugacity of magma (Liou, 1973; Sial et al., 1999). BmG outcrop at the northeastern part of the Fomopéa granitic complex and elsewhere cross-cut BHG in form of veins. The contacts between BHG and BmG is always sharp, pointing that BmG was emplaced after the crystallization of BHG. BmG are fine- to medium-grained and heterogranular, with biotite, zoned plagioclase, K-feldspar (microcline) and quartz. Accessory minerals include Fe–Ti oxides, apatite, zircon and ± titanite. EsG seem to be the last emplaced granite unit in the Fomopéa pluton; it cross-cuts only BHG and displays no structural relationship with BmG. Rocks are greyish to leucocratic, medium-grained and heterogranular. The most frequent mineral association is K-feldspar, albitic plagioclase and green sub-euhedral to euhedral edenite. Accessory minerals include Fe–Ti oxides, titanite and apatite. All rocks are chemically calc-alkaline; BHG is metaluminous and BmG and EsG are metaluminous to weakly peraluminous. BmG and EsG are felsic I-type granitoids, whereas BHG correspond to mafic I-type granitoids. Mafic enclaves as well as gneiss xenoliths are recognized in the field. Kwékam et al. (2009) provide U–Pb dates on zircons from two samples: K204, a dioritic stock in BHG, and K104, a proper granitoid from BHG (location of samples in Fig. 2b), yielding Pan-African ages of 623–613 Ma. These authors also obtained a Rb–Sr whole rock isochron age of 572 ± 48 Ma for the BHG unit. All these recent ages will be discussed hereafter at the light of the new structural data.

The Fomopéa granitic pluton intruded a high-grade basement mainly made of banded gneisses and subordinate amphibolites. It is limited at the southeastern edge by the ductile Fotouni–Fondjomekwet mylonitic zone (FFMZ: Fig. 2a). The banded gneisses are greyish medium- to coarse-grained with dark layers composed of amphibole, plagioclase, biotite, titanite, magnetite and apatite, and white layers made of quartz, K-feldspar and plagioclase. Amphibolites are darkish and fine-grained. The most frequent minerals are amphibole, plagioclase and biotite. Titanite, magnetite and apatite are accessory minerals. The FFMZ is made up of protomylonites and mylonites. Protomylonites belong to the pluton body; they are medium- to coarse-grained with quartz, K-feldspar, plagioclase and chlorite, corresponding to the deformation of the plutonic rocks in greenschist facies conditions. Mylonites are greyish, or sometimes leucocratic, banded, fine-grained, with quartz, K-feldspar, biotite, plagioclase, garnet, muscovite, cordierite, sillimanite and monazite. Their mineral composition is indicative of a metapelite protolith, that underwent mylonitization under mid-pressure amphibolite facies conditions.

3. Materials and methods

Today, measurement of Anisotropy of Magnetic Susceptibility (AMS) is the most efficient method to determine petrofabric orientation in rocks, even in rocks that are visually isotropic.

Oriented cylinder samples were taken from 112 different stations (Fig. 2b) distributed among the three mean lithological granite formations: 14 stations from edenite syenogranites (EsG), 29 stations from biotite monzogranites (BmG) and 56 stations from biotite-hornblende granites (BHG). The 13 others stations are obtained from the gneissic or amphibolitic country rocks (8 stations) and mylonites (5 stations). Two or three oriented cores were collected per station. Each core yielded at least two cylindrical samples, hence providing four (or more) samples per station. A total of 521 samples were analyzed in this study. Each individual sample is 22 mm in length and 25 mm in diameter, the standard size for magnetic measurements. All samples were measured for AMS in LMTG (Laboratoire des Mécanismes et Transferts en Géologie; Toulouse, France) using a Kappabridge susceptometer (KLY-3S, Agico, Czech Republic) working at a low alternating inductive field ($\pm 4 \times 10^{-4}$ T, 920 Hz) with a sensitivity of about 2×10^{-7} SI, allowing anisotropy discrimination below 0.2% over a wide range of susceptibility. AMS is a second-rank tensor expressed by its principal eigenvectors and eigen values $K_{max} = K_1 > K_{int} = K_2 > K_{min} = K_3$, respectively representing the maximum, intermediate and minimum axes of the magnetic susceptibility ellipsoid.

The bulk magnetic susceptibility magnitude is given by $Km = (K_1+K_2+K_3)/3$. The long axis of the ellipsoid, K_1, defines the magnetic lineation and the short axis, K_3, defines the pole of the magnetic foliation (the plane formed by K_3 and K_2 axes). In plutonic rocks, the magnetic fabric is usually coaxial with the mineral fabric. When a granite has a so-called "paramagnetic" behaviour, K_3 represents the pole of the foliation marked by the preferred orientation of the main Fe-bearing silicate mineral, namely biotite, and K_1 represents the biotite lineation defined as the axis of rotation, or zone axis, of the biotite foliation (Bouchez, 2000). It is worth to notice that, in these rocks, very small quantity of ferrimagnetic material may be present as tiny inclusions in silicate minerals (Pignotta and Benn, 1999). According to Grégoire et al. (1998), when a granite has a ferrimagnetic or ferromagnetic (sensu lato) behaviour (i.e. magnetite-bearing granites), K_3 defines the pole of the average flattening plane and K_1 the elongation direction of the shape preferred orientation of magnetite. Therefore, whatever the case, foliations and lineations, obtained by magnetic means, can be used as indicative of the mineral fabrics.

Table 1
Anisotropy of low-field magnetic susceptibility for the Fomopéa granitic pluton. K_1, K_2 and K_3 are the maximum, intermediate and minimum susceptibility intensities respectively; $Km = (K_1+K_2+K_3)/3$ is the mean magnetic susceptibility; L% is the linear anisotropy percentage ($L\% = 100 \times [(K_1/K_2)-1]$); F% is the planar anisotropy percentage ($F\% = 100 \times [(K_2/K_3)-1]$), P% is the total anisotropy percentage ($P\% = 100 \times [(K_1/K_3)-1]$); $T = [2\ln(K_2/K_3)/(\ln(K_1/K_3)]-1$ is the Jelinek's shape parameter (Jelinek, 1981); Dec: declination in degrees; Inc: inclination in degrees.

Site	Lon (E) (°)	Lat (N) (°)	Mean AMS parameters					Mean eigenvectors					
			Km (microSI)	L%	F%	P%	T	K1		K2		K3	
								Decl	Incl	Decl	Incl	Decl	Incl
Biotite-hornblende granites													
TN2	10.15	5.32	12 671	14	23	40	0.23	148	38	250	15	357	48
TN17	10.12	5.32	13 946	14	17	34	0.10	62	30	156	7	259	59
TN18	10.13	5.32	6604	2	8	10	0.58	308	3	38	15	207	75
TN20	10.13	5.34	27 475	7	26	35	0.53	85	27	184	18	303	57
TN21	10.14	5.35	5557	5	2	7	−0.35	10	7	107	43	272	46
TN22	10.14	5.36	15 650	7	26	35	0.53	82	49	176	4	270	40
TN23	10.14	5.36	3142	3	3	6	−0.10	210	15	109	34	320	52
TN24	10.15	5.37	10 706	12	17	31	0.18	110	32	200	0	291	58
TN25	10.16	5.35	9563	1	20	22	0.85	206	44	24	46	115	1
TN28	10.14	5.34	4878	14	3	17	−0.67	143	49	238	4	331	41
TN29	10.14	5.33	20 620	12	29	44	0.37	11	30	108	12	218	58
TN30	10.13	5.33	5471	9	10	21	0.05	78	23	175	14	294	62
TN31	10.14	5.39	23 066	2	30	32	0.86	201	6	108	27	302	62
TN32	10.15	5.39	15 834	2	25	27	0.84	217	4	108	77	308	13
TN33	10.15	5.40	31 095	15	30	50	0.31	6	16	106	31	252	54
TN34	10.16	5.39	18 638	51	7	61	−0.72	327	0	237	45	57	45
TN35	10.15	5.38	8704	3	19	23	0.70	162	12	64	34	268	53
TN36	10.14	5.38	7443	5	16	21	0.53	30	12	137	53	292	34
TN37	10.15	5.38	2288	3	17	20	0.68	80	37	187	21	300	45
TN38	10.15	5.37	22 796	1	36	38	0.92	180	6	273	29	80	60
TN39	10.17	5.37	12 382	8	29	39	0.54	118	37	216	10	319	51
TN40	10.13	5.31	32 171	2	36	39	0.88	169	7	75	25	273	63
TN41	10.15	5.31	2146	7	3	10	−0.42	147	27	263	41	35	37
TN42	10.15	5.33	35 953	11	51	67	0.60	133	7	223	5	347	82
TN43	10.16	5.32	380	1	1	1	−0.04	77	33	347	1	255	57
TN44	10.15	5.34	5718	2	8	10	0.63	2	6	96	38	264	52
TN45	10.16	5.35	7161	6	4	9	−0.20	78	19	339	25	201	57
TN46	10.15	5.37	16 706	7	41	50	0.69	48	33	153	22	270	49
TN47	10.15	5.33	8024	6	1	6	−0.74	43	12	150	56	305	31
TN48	10.16	5.36	4336	2	15	16	0.80	226	3	133	41	319	48
TN49	10.16	5.36	8504	8	14	23	0.27	347	67	84	3	176	23
TN50	10.17	5.35	19 910	5	14	20	0.49	39	1	130	13	307	77
TN51	10.18	5.35	14 598	13	25	41	0.28	273	46	111	42	12	9
TN55	10.20	5.37	9266	16	20	39	0.12	64	24	161	15	280	61
TN56	10.19	5.36	11 965	11	23	36	0.32	65	23	317	36	180	45
TN57	10.19	5.37	12 755	25	18	47	−0.15	50	20	144	10	260	67
TN59	10.17	5.38	13 515	11	28	42	0.41	86	49	215	29	321	27
TN62	10.20	5.38	11 889	30	7	39	−0.59	23	14	278	45	126	42
TN69	10.12	5.28	1434	4	7	11	0.20	201	6	299	52	106	37
TN72	10.17	5.34	695	6	7	13	0.10	32	24	163	56	291	23
TN75	10.23	5.39	8294	8	9	18	0.09	346	18	201	68	80	12
TN77	10.23	5.39	9794	6	4	10	−0.13	76	4	345	22	175	68
TN78	10.23	5.38	474	1	1	2	−0.01	301	24	115	66	210	2
TN80	10.22	5.38	9587	4	0	4	−0.88	66	5	193	82	335	6
TN81	10.20	5.37	9831	5	4	9	−0.10	69	34	178	25	296	45
TN82	10.21	5.37	6947	7	13	20	0.32	91	15	350	36	199	50
TN93	10.20	5.42	4077	3	10	13	0.51	217	1	307	22	125	68
TN96	10.22	5.43	8703	3	18	22	0.70	287	1	197	3	44	87
TN101	10.13	5.38	9964	7	39	48	0.66	115	38	21	5	284	52
TN102	10.12	5.35	6027	3	43	48	0.84	93	23	0	7	254	65
Biotite monzogranites													
TN3	10.20	5.42	3973	3	15	18	0.67	88	31	183	8	285	58
TN19	10.14	5.34	5056	4	11	15	0.50	83	30	182	15	296	56
TN26	10.15	5.35	37 078	3	12	15	0.64	301	2	32	22	206	67
TN27	10.14	5.34	5942	14	6	21	−0.37	40	2	130	12	301	78
TN54	10.18	5.37	4998	2	6	8	0.50	185	10	276	5	31	79
TN58	10.18	5.37	9225	10	28	41	0.46	95	24	195	22	323	57
TN60	10.19	5.38	5298	5	13	19	0.40	49	11	144	22	295	66
TN61	10.20	5.40	8535	7	17	25	0.40	70	26	170	19	292	57
TN63	10.19	5.39	2700	5	9	15	0.33	51	1	142	7	310	83
TN64	10.19	5.40	15 159	8	37	48	0.59	45	7	139	30	303	59
TN65	10.20	5.40	6993	6	20	27	0.54	85	48	353	1	262	42
TN74	10.24	5.40	2670	5	1	6	−0.64	347	23	191	65	81	9
TN76	10.24	5.39	3611	4	3	7	−0.09	55	2	145	18	319	72
TN79	10.22	5.38	1940	3	11	15	0.54	57	13	326	3	222	76
TN84	10.22	5.39	11 263	9	10	20	0.06	21	68	245	16	151	14
TN85	10.20	5.42	133	1	4	5	0.51	60	9	160	49	322	40

Table 1 (*continued*)

Site	Lon (E) (°)	Lat (N) (°)	Mean AMS parameters					Mean eigenvectors					
			Km (microSI)	L%	F%	P%	T	K1		K2		K3	
								Decl	Incl	Decl	Incl	Decl	Incl
TN86	10.20	5.42	1799	5	7	12	0.19	49	12	144	25	295	62
TN87	10.20	5.42	10 937	8	26	36	0.49	58	17	152	14	278	68
TN88	10.21	5.42	8162	7	19	28	0.43	64	8	156	14	305	73
TN89	10.20	5.42	5318	8	16	26	0.32	66	18	160	12	283	68
TN90	10.22	5.41	8667	16	13	31	−0.08	77	13	171	18	312	68
TN91	10.24	5.40	1848	3	6	9	0.39	356	1	87	25	263	65
TN92	10.23	5.40	7965	6	8	15	0.12	60	7	152	12	300	76
TN94	10.21	5.43	7410	8	16	25	0.30	110	13	200	1	294	77
TN95	10.21	5.41	5821	9	20	31	0.34	71	15	165	14	297	69
TN98	10.25	5.41	11 468	1	22	23	0.91	242	0	152	3	332	87
TN99	10.25	5.42	10 709	3	18	22	0.71	53	2	143	14	316	76
Edenite syenogranites													
TN1	10.11	5.33	1106	8	1	9	−0.70	111	23	336	59	210	20
TN5	10.11	5.33	5203	12	2	15	−0.65	100	5	9	11	216	78
TN6	10.12	5.32	807	9	1	10	−0.82	91	20	349	30	210	53
TN7	10.10	5.32	2379	7	3	10	−0.41	108	15	6	37	216	48
TN8	10.11	5.34	11 496	15	11	28	−0.13	96	21	192	15	316	64
TN9	10.12	5.34	53 281	24	15	44	−0.21	112	43	357	24	247	37
TN10	10.11	5.33	39 540	5	27	34	0.65	305	4	211	48	38	42
TN11	10.11	5.33	8438	24	0	25	−0.97	76	2	345	35	168	55
TN12	10.11	5.34	57 922	28	42	82	0.17	93	21	0	6	255	68
TN13	10.10	5.33	4492	11	6	18	−0.26	100	16	7	10	245	71
TN14	10.10	5.31	356	1	3	3	0.46	130	23	18	41	241	40
TN15	10.11	5.32	2300	9	4	14	−0.35	105	19	199	9	313	69
TN16	10.11	5.30	3248	1	4	4	0.73	226	75	322	1	52	15
TN103	10.10	5.32	3965	14	7	22	−0.28	314	28	216	14	102	58
TN104	10.09	5.32	951	6	2	8	−0.53	100	11	333	73	193	14
TN105	10.09	5.33	9537	19	10	31	−0.28	109	13	14	19	231	67
Basement rocks													
TN66	10.17	5.30	34	4	11	16	0.46	48	22	185	62	311	18
TN68	10.12	5.27	14	1	9	10	0.84	48	28	200	59	311	12
TN70	10.14	5.27	325	7	10	18	0.18	33	11	259	75	125	11
TN71	10.22	5.34	379	3	12	15	0.58	49	2	147	72	318	18
TN73	10.20	5.34	11 877	19	15	37	−0.11	233	15	40	74	143	4
TN100	10.13	5.39	21 153	8	29	39	0.55	129	46	352	35	245	23
TN107	10.11	5.37	762	5	17	22	0.55	46	5	138	21	303	68
TN108	10.16	5.41	19 864	4	27	33	0.70	147	23	46	24	275	56

The raw magnetic data for each of the 112 stations concerning the Fomopéa granitic pluton are reported in Table 1, successively giving the station, the geographical location, the main AMS parameters such as: bulk susceptibility magnitude (Km), the linear anisotropy percentage ($L\% = 100 \times [(K_1/K_2)-1]$), the planar anisotropy percentage ($F\% = 100 \times [(K_2/K_3)-1]$), the total anisotropy percentage ($P\% = 100 \times [(K_1/K_3)-1]$), the T-shape parameter of Jelinek (1978) ($T = (2\ln(K_2/K_3)/\ln(K_1/K_3))-1$); the declination and inclination of maximum, intermediate and minimum eigenvectors, i.e. K_1 (magnetic lineation), K_2 and K_3 (pole to the magnetic foliation).

The thermomagnetic curves were obtained using a CS2 apparatus coupled to the KLY-2 Kappabridge instrument (Agico, Czech Republic). Hysteresis measurements at room temperature were performed in "Geological Survey of Canada-Pacific paleomagnetism laboratory" using a vibrating sample magnetometer (VSM).

4. Magnetic susceptibility and magnetic mineralogy

4.1. Magnetic susceptibility

The magnetic susceptibility magnitudes of the whole collection, expressed by Km in SI units, vary greatly over the Fomopéa massif from 133×10^{-6} to $57\,922 \times 10^{-6}$ SI (Table 1; Fig. 3a). These values indicate the presence of both (1) ferromagnetic behaviour (Km $> 500 \times 10^{-6}$ SI) dominated by the signal of magnetite that represents 96% of the stations and (2) paramagnetic behaviour (Km usually less than 500×10^{-6} SI; Fig. 3b) dominated by the signal of iron-bearing silicates (Rochette, 1987; Bouchez, 2000) that represents only 4% of the stations. Ferromagnetic and paramagnetic behaviours appear in the same petrographic group and even, sometimes, in the same station, indicating an uneven distribution of magnetite in some samples. Km values range from 380×10^{-6} to $57\,922 \times 10^{-6}$ for BHG, from 133×10^{-6} to $37\,078 \times 10^{-6}$ for BmG and from 356×10^{-6} SI to $39\,540 \times 10^{-6}$ for ESG. In the banded amphibole gneisses and amphibolites, Km values range from 345×10^{-6} to $57\,084 \times 10^{-6}$ SI. Low susceptibility magnitudes from 14×10^{-6} to 379×10^{-6} SI corresponding to a paramagnetic behaviour are especially noted in mylonitic rocks to the southeast. Sample TN 73 belonging to the Fomopéa pluton, but deformed at the contact with the mylonitic zone, has a much higher susceptibility magnitude in the same range than other granitoid samples. Conversely, the stations showing high to very high ($>15 \times 10^{-3}$ SI, i.e. $> 15\,000 \times 10^{-6}$ SI) magnetic susceptibility magnitudes are mainly located within a N–S striking band, and are mainly enclosed in the BHG unit.

4.2. Magnetic mineralogy

4.2.1. Susceptibility vs temperature

Thin sections allow to observe different types of opaque minerals (1) fine- to medium-grained oxides included in amphibole, biotite and feldspar; (2) free intercrystalline coarse-grained opaque minerals. Measurements of continuous low-field thermomagnetic curves (*K–T* curves: normalized susceptibility

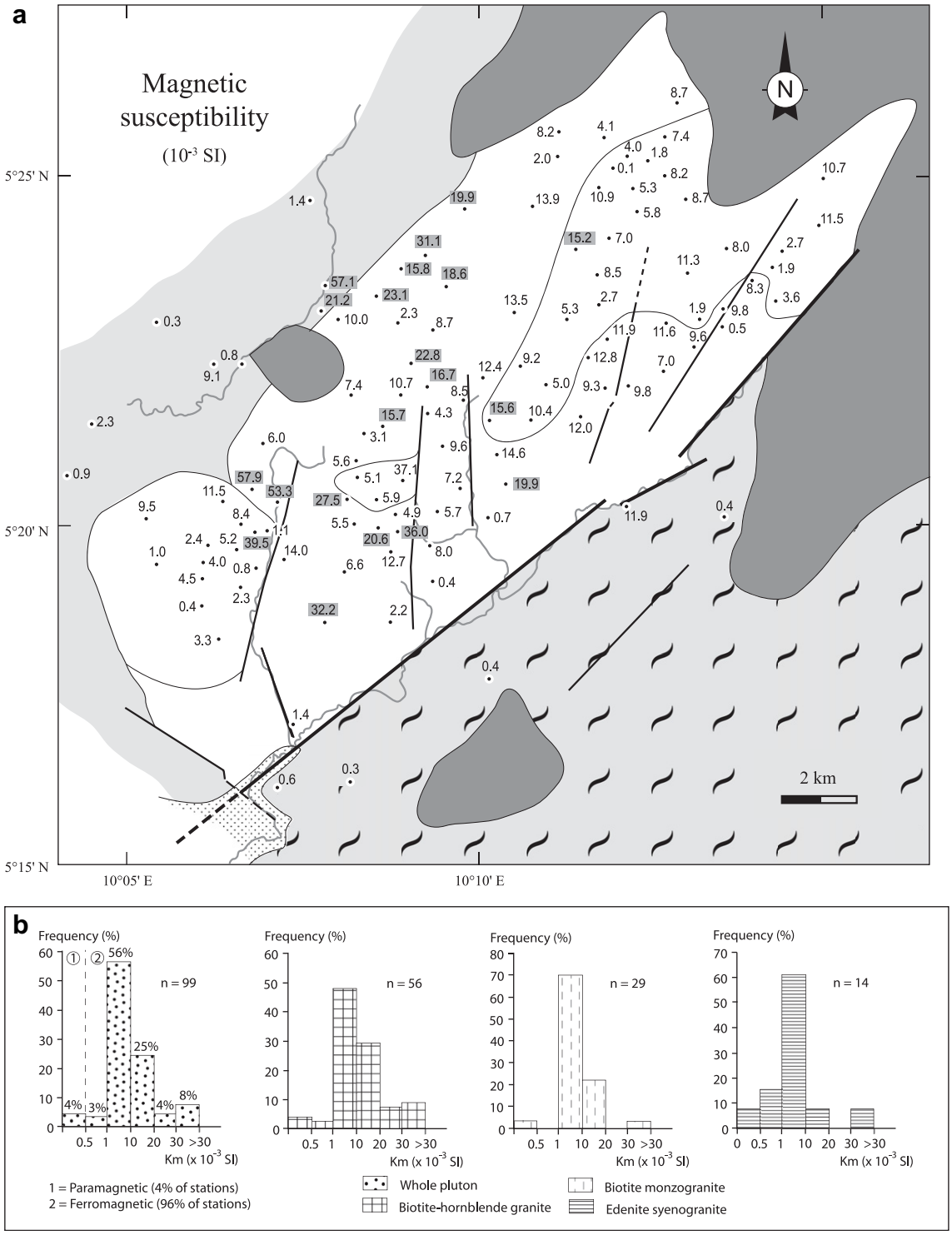

Fig. 3. (a) Susceptibility (Km) map in 10^{-3} SI of Fomopéa granitic pluton; values $> 15 \times 10^{-3}$ SI are shaded. (b) Susceptibility histogram.

vs temperature) confirm that magnetite is the main susceptibility carrier, as suggested by the high susceptibility magnitudes. Representative examples of these curves are shown in Fig. 4a–c for the three petrographic groups of Fomopéa granitic pluton. Progressively, samples were heated up to 700 °C and cooled to room temperature. Most of these curves have a regular shape in both heating and cooling cases and they display a decrease in the intensity of susceptibility at 570 °C (Fig. 4a–c) indicating the presence of pure magnetite as the main carrier of the magnetic susceptibility. This is consistent with the high susceptibility values and mineral compositions witnessing the oxidized nature of the magmas. A slight decrease at ca 350 °C in the heating curve suggests the presence of some maghaemite, because the cooling curve is always devoid of any perturbation. The magnetic phases evidenced by *K–T* curves are the same in the three mean petrographic groups of Fomopéa granitic pluton, hence there is no difference in the magnetic carriers in those petrographic groups.

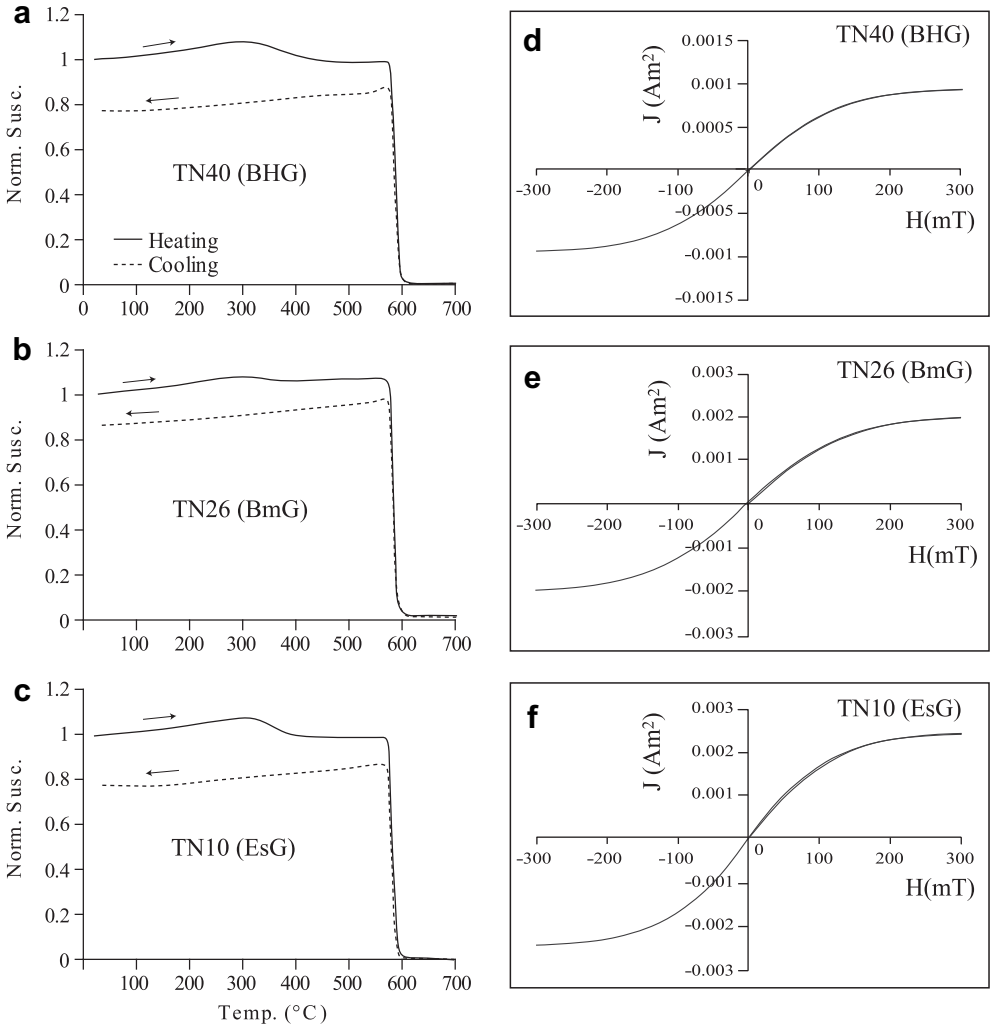

Fig. 4. (a–c) *K–T* curves (susceptibility vs temperature) for representative samples (TN40 for BHG, TN26 for BmG and TN10 for EsG). M is magnetization in Am^2 and H is applied field in mT; (d–f) Representative hysteresis loops for the same samples.

4.2.2. Hysteresis

Some typical hysteresis loops from representative samples of the three petrographic groups are shown in Fig. 4d–e. The hysteresis curves and hysteresis parameters reveal the existence of pure magnetite and all studied samples plot in the multidomain (MD) field of the Day et al. (1977) diagram (not shown). This distribution is consistent with the existence of coarse-grained magnetite, as previously described in thin sections.

5. Structures and microstructures

Deformation in granitic rocks can take place in the magmatic state or in the solid state at high-, moderate- or low-temperatures. It is responsible for foliations and lineations and the relevant microstructures can be recognized in thin sections. Typical microstructural features are shown in Fig. 5. Four types of microstructures (magmatic texture, incipient solid-state deformation, localised bands of deformation, pervasive mylonitic deformation) have been observed in thin sections (Fig. 5). Magmatic textures were observed at some places in BHG (Fig. 5a) and ESG. They also characterize the (monzo)dioritic stocks (Fig. 5b). However, in the whole pluton, the microstructures are generally indicative of incipient solid-state deformation in near solidus conditions, as evidenced by the presence of small recrystallized quartz grains (Fig. 5c).

Localized bands of deformation characterize the BHG unit (Figs. 5d–f, and 6). They were observed in the field in stations that show N–S striking magnetic foliations and N–S trending magnetic lineations. They correspond to vertical microfaults or shear zones, where minerals are broken, denoting a high strain deformation at low to medium temperatures. Although these N–S structures sometimes correspond to deformation in higher temperature conditions, strain remained always localized to a zone of no more than about 2 mm to a few centimetres wide. The sense of motion is sinistral (Fig. 5e). It is also worth to notice that the highest susceptibilities were observed in the area, where the localised N–S deformation bands are common (see Fig. 3), suggesting that this style of deformation may coincide with a higher amount of iron-bearing mineral, such as secondary magnetite or secondary epidote (indeed observed in thin section).

S/C structures are commonly observed in the mylonitic zone (Fig. 5g–h). They are consistent with a dextral sense of motion, also confirmed by typical sigma-type porphyroclasts and their crystallization tails.

6. AMS data

Projection diagrams of magnetic fabrics determined from AMS for all the sampled stations in Fomopéa granitic pluton

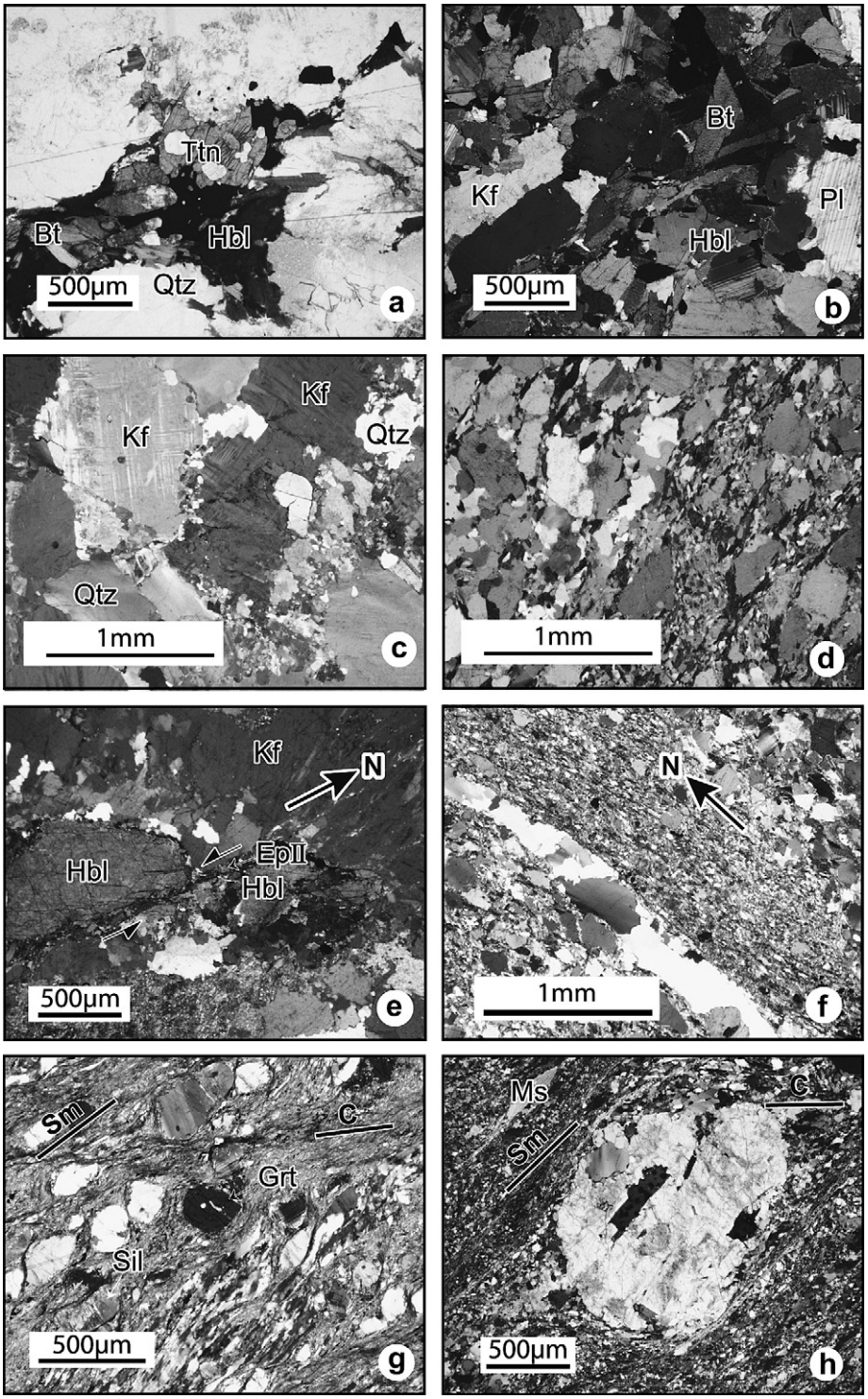

Fig. 5. Microphotographs (crosssed polars) of typical microstructures : (a) magmatic texture in biotite-hornblende granite (TN33); (b) magmatic texture in biotite monzodiorite (TN103); (c) incipient solid-state deformation in biotite monzogranite (TN27); (d–f) localized NS sinistral bands of deformation in biotite-hornblende granites (respectively TN 40, TN45 and TN42); (h, i) mylonitic textures with Sm (foliation) and C (shear plane) showing a dextral sense of motion in the southeastern mylonites (respectively TN71 and TN66). Bt : biotite, EpII: secondary epidote, Grt: garnet, Hbl: hornblende, Kf: K-feldspar, Ms: muscovite, Sil: sillimanite, Ttn: titanite.

and its country rocks generally display no scattering of the magnetic data. In addition, the consistency with the field observations was checked when possible, as in the mylonites for instance. Hence, the magnetic foliations and lineations are regarded as respectively coaxial with the mineral foliations and lineations.

6.1. Anisotropy of magnetic susceptibility

The total anisotropy percentage (P%) varies from 1% to 82% (Table 1; Fig. 7). According to Rochette et al. (1992) and Bouchez (1997, 2000), P% values lower than 15% in granites correspond to magnetite-free rocks (also characterized by low Km values). In

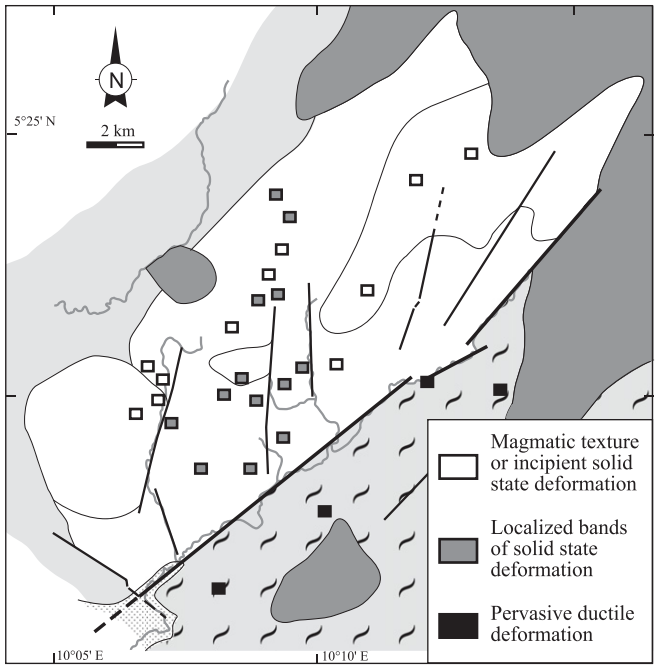

Fig. 6. Distribution of microstructures in Fomopéa pluton.

Fomopéa granites, P% is highly variable among the three petrographic groups. It varies from 1% to 82% in BHG, from 5% to 48% in BmG and from 3% to 34% in EsG. Such high variability of anisotropy values precludes the use of P% as a quantitative strain intensity indicator, as it is more linked to the magnetite distribution in rocks than to the strain itself. This is supported by the roughly linear relationship between Km and P%, on the P% vs Km diagram (Fig. 7). Nevertheless, the highest anisotropies are observed either near external or internal contacts in the pluton, or in the zones associated with the N–S deformation bands.

In banded gneisses, anisotropy values vary from 9% to 50%. Finally, it should be noted that anisotropies are very homogeneous (13% on average) in the paramagnetic mylonites of FFMZ. Although lesser than in the pluton, the magnetic anisotropies of the mylonites are rather high for magnetite-free (i.e. low susceptibility) rocks (P% = 11–18%). They characterize the lattice fabric of minerals that was acquired during ductile deformation and dynamic recrystallization. Such (relatively) high values confirm that the rocks were subjected to a rather intense deformation, leading to strong preferred orientations of the iron-bearing silicates (mainly biotite). By comparison, the TN 73 protomylonite has a very low anisotropy degree (P% = 4%), that witnesses the incomplete reorientation of the rocks and the likely superposition of two different and diachronous fabrics.

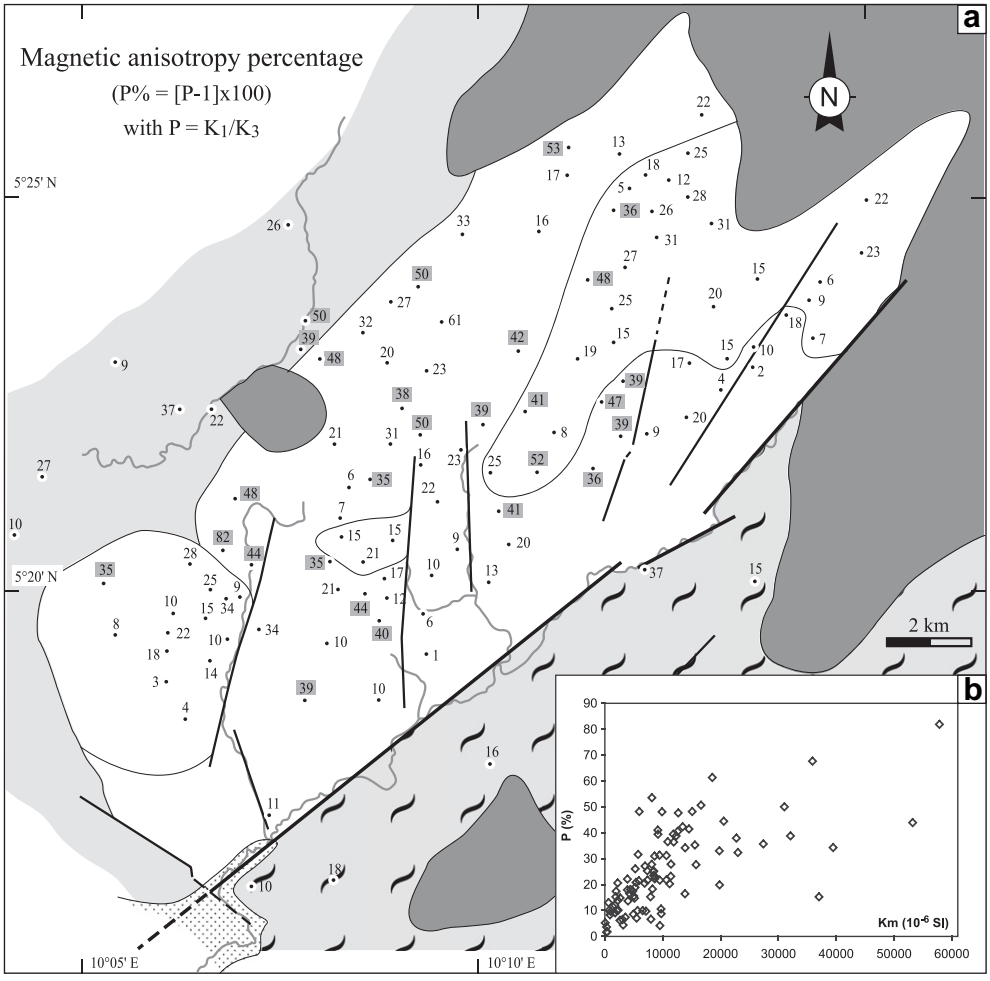

Fig. 7. (a) Anisotropy percentage ($P\% = 100 \times [(K_1/K_3)-1]$) map of Fomopéa granitic pluton. Values ≥ 35% are shaded; (b) P% vs Km diagram.

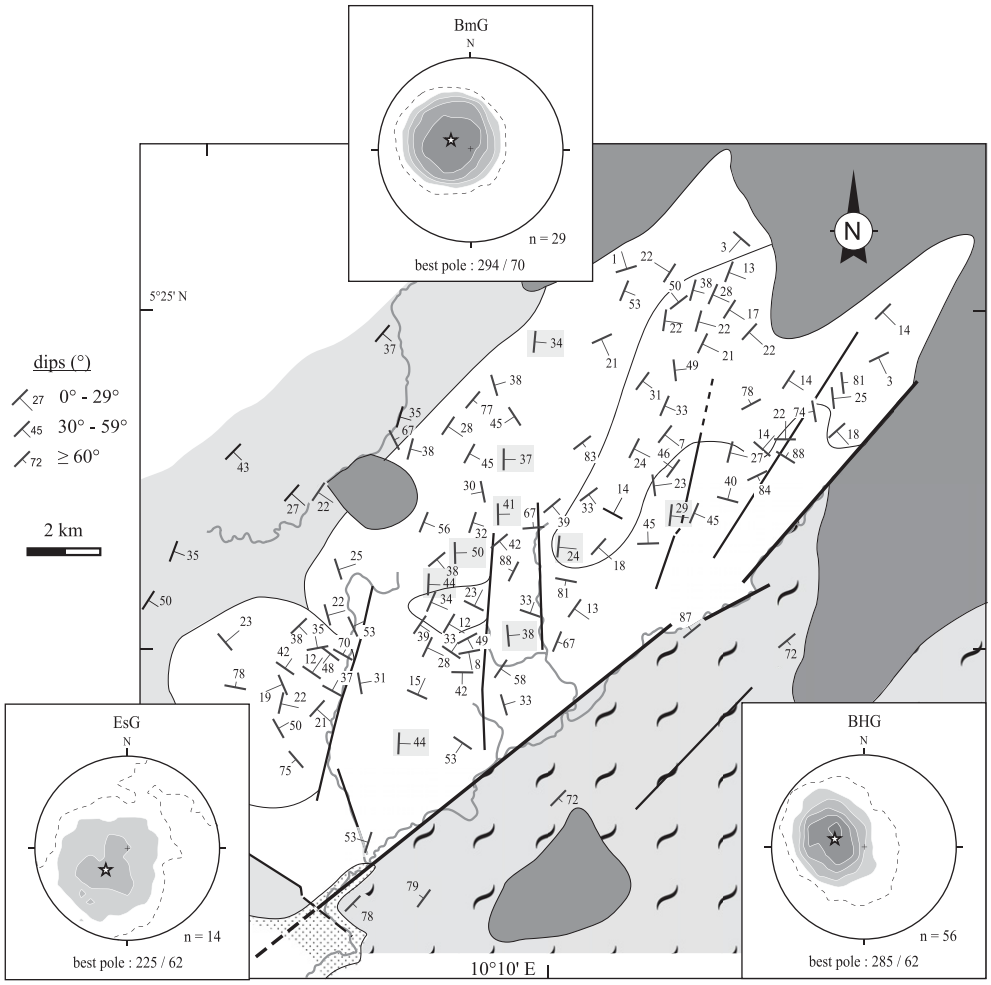

Fig. 8. Magnetic foliation map and projection diagrams for foliation poles (lower hemisphere, contour intervals = 2%); shaded symbols correspond to N–S striking foliations.

The linear anisotropy percentage, L%, also presents a high variability among the petrographic groups (Table 1). It varies from 1% to 51% in BHG, from 1% to 16% in BmG and from 1% to 24% in EsG. In the gneisses, it varies from 1% to 12% and in the mylonites it varies from 3% to 19%. The planar anisotropy percentage (F%) displays the same behaviour as the two other parameters. BHG show the largest variation from 0% to 51%, whereas in BmG it varies from 3% to 37% and in EsG from 0% to 27%. In the gneisses, it varies from 7% to 36%. In the mylonites, the planar anisotropy percentage is more homogeneous and varies from 9% to 15%.

The Jelinek's (1981) shape parameter (T) of the AMS ellipsoid is presented in Table 1. The whole pluton shows about 55% of stations with a triaxial shape ($T \approx 0$) ellipsoid, while more than 34% of stations show an oblate shape ($T > 0$) ellipsoid and only 11% of sites a prolate shape ($T < 0$). This variation of shape of the ellipsoids is valid in the same range for BHG (54%, 38% and 9% respectively) and BmG (67%, 33% and 0% respectively). The EsG is slightly different with the different T value ranges representing 57%, 29% and 14% respectively. Although ellipsoid shapes are not strain intensity indicators, it is noticeable that oblate ellipsoids are observed along the N–S strain zone in BHG, on the northern edge of the pluton and in banded gneisses and amphibolites in country rocks.

6.2. Magnetic foliations

Magnetic foliations (Fig. 8) are generally parallel to the foliations measured in the field. Azimuths and plunges of the magnetic foliation poles are variable, but projections of BHG and BmG foliation poles plot in the same area of the diagram with respective best poles at 285/62 and 294/70 (Fig. 8). The magnetic foliations have generally gentle to moderate dips. BHG shows 26% dips between 0° and 30°, 57% between 30° and 60° and 17% between 60° and 90°. In BmG, we have respectively 74%, 26% and 0% (more than 93% of stations have foliations dipping less than 40°) and in EsG, we have 36%, 43% and 21% respectively. Average strikes vary slightly depending of rock units. In BHG and BmG, most strikes cluster around the NNE direction and, in EsG, 77% of strikes cluster around the NW direction. The mylonites display noticeable subvertical magnetic foliations in agreement with field observations.

6.3. Magnetic lineations

The magnetic lineations K_1 present mostly low plunges (<30° for 79% of the stations; Fig. 9) for the whole pluton. They are also rather homogeneous in individual petrographic rock types. In BHG, 69% of the stations display plunges between 0° and 30° (93% in BmG and 92% in EsG), and 30% display plunges between 30° and 60°. Their trends are well organised in each rock type (NE–SW in BmG, NW–SE in EsG). In BHG, NS-trending magnetic lineations correspond to stations that also show N–S strikes of their magnetic foliations (grey-shaded symbols in Figs. 8 and 9) and that correspond to solid-state deformation along discrete N–S corridors. The progressive rotation to the north of earlier east-trending lineations

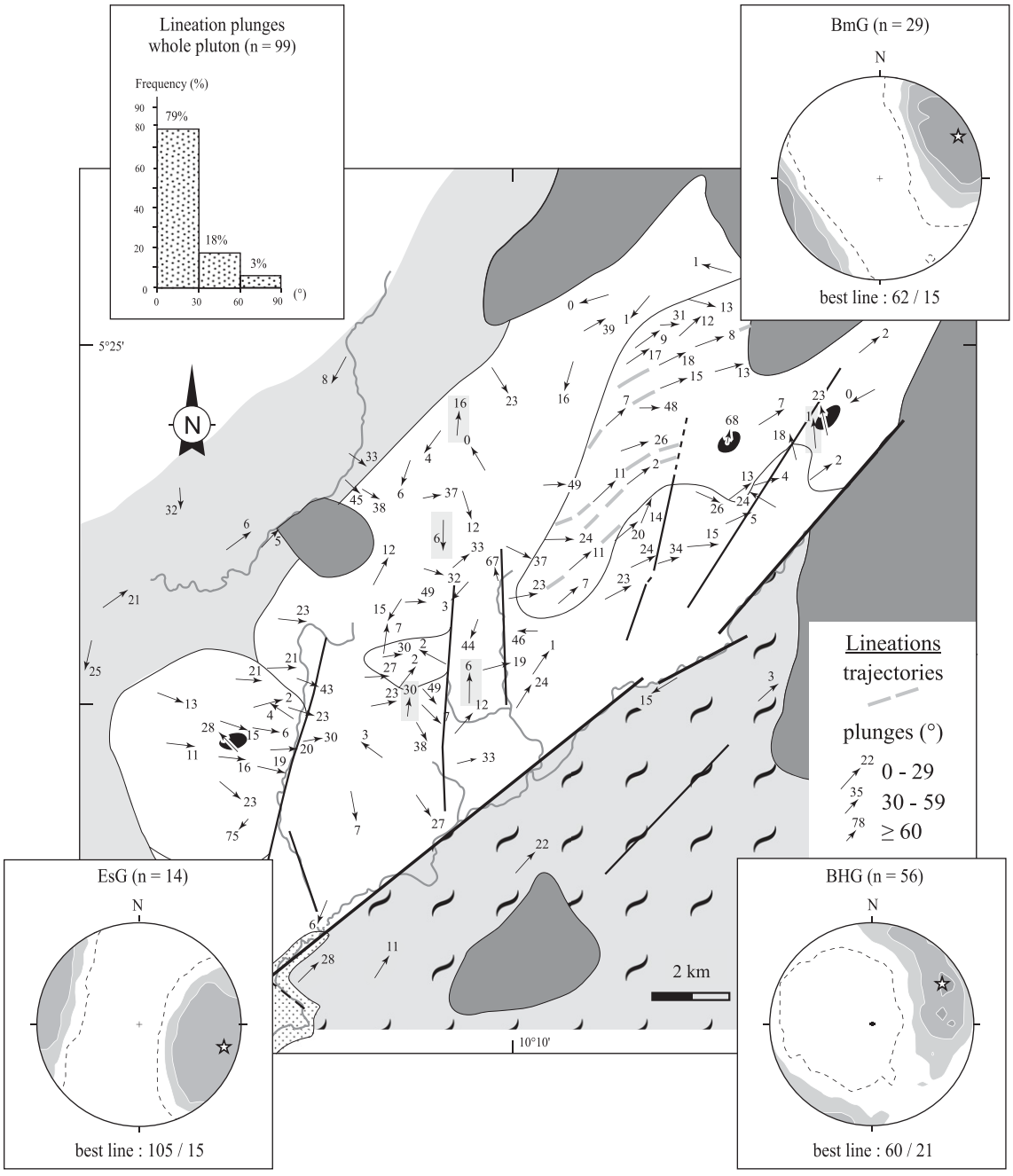

Fig. 9. Magnetic lineation map and corresponding projection diagrams (lower hemisphere, contour intervals = 2%); shaded symbols correspond to N–S trending lineations.

is evidenced in the projection diagram of BHG (Fig. 9). In addition, the lineation trajectories in BmG suggest a sinistral sense of motion along a N–S magmatic shear zone. Once again, EsG rocks display different orientations with no evidence of rotation. Lineations in the mylonites are subhorizontal and trend NE–SW, pointing to a mainly transcurrent motion along the FFMZ.

7. Discussion

7.1. Interpretation of the plutonic fabrics

Plutonic fabrics are regarded either as related to magma emplacement or resulting from tectonic strain after emplacement. Actually, emplacement-related fabrics (e.g. magmatic microstructures and steep lineations: Clemens et al., 1997; Razanatseheno et al., 2009) are rarely preserved, because they are easily overprinted by minor ductile strain during or after cooling of the magma. Such overprinted fabrics may often be observed in the whole pluton, or only in some places, a rather common case, where microstructural interpretation will play a major role (e.g. Nascimento et al., 2004; Benn, 2009, and references therein).

N–S striking sinistral deformation bands mostly concerns the BHG. Microstructural observations point to their development in sub-solidus conditions and during a continuum from high to low-temperatures conditions. Therefore, the chronology and interpretation of the fabric acquisition is suggested as follows. BHG magmas were emplaced first, likely with an ENE–WSW stretching direction that may reflect the tectonic strain at that time (D1 in Fig. 10). Emplacement of the BmG magmas followed. Because these rocks display a sigmoidal or flexural rotation of their magmatic structures

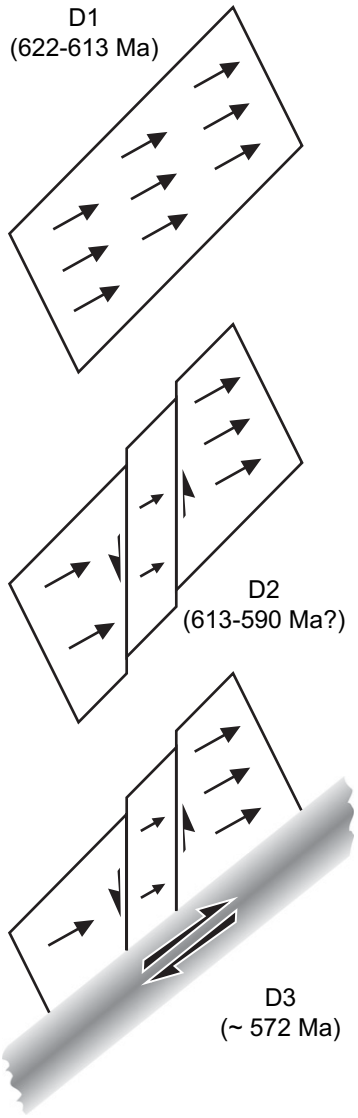

Fig. 10. Tectonic history of Fomopéa pluton.

along a N–S to NNE–SSW plane (Fig. 9), but are devoid of significant solid-state deformation, they may have been emplaced at the time when the already crystallized BHG underwent localized solid-state deformation along the N–S corridors. This deformation corresponds to a sinistral sense of motion (D2). This phase was also responsible for the development of secondary minerals, including secondary magnetite in the N–S deformation bands of BHG, as can be seen from petrographic observations and from the distribution of the highest susceptibility values. Emplacement of the EsG magmas with an ESE–WNW stretching direction likely occurred later, but its timing is difficult to establish because of the lack of geochronological data. Development of the shear zone and mylonites along the southern border of Fomopéa pluton witness dextral transcurrent tectonics that occurred well after, because the shear zone cross-cut the N–S corridors and left a low grade imprint along the southeastern border of the pluton.

7.2. Discussion of ages and geodynamic implications

The geological history of the area will be considered with respect to the different phases of deformation recognized in the Fomopéa granitic complex as well as the ages obtained by Kwékam et al. (2009), and other ages and structural data from Cameroon and eastern Nigeria. In the gneissic country rocks, magnetic foliations strike NE–SW with low to medium dip towards the SE, and magnetic lineations are mostly subhorizontal. In the present state of knowledge, these structures are regarded as Pan-African, but may have been acquired before the emplacement of Fomopéa pluton. It has not been possible to relate them to a precisely dated phase so far. An isolated age of ca 648 ± 5 Ma found for one zircon of the K204 dioritic stock in Fomopéa may have been inherited from the country rocks (Kwékam et al., 2009) possibly dating this earlier phase.

Kwékam et al. (2009) also obtained well-defined U–Pb zircon ages ranging from 623 to 613 Ma from rocks in the BHG unit of the Fomopéa pluton. The older ages at 621 ± 3 Ma and 623 ± 2 Ma are respectively derived from one zircon belonging to a dioritic stock (K204) and from two zircons belonging to a proper BHG granitoid (K104). Taken together, both samples yield an age of 622 ± 4 Ma, that is retained by Kwékam et al. (2009) as the age of BHG emplacement. A younger (613 ± 2 Ma) age is also obtained from two other zircons of the (K104) BHG granitoid. The time span between 623 and 613 Ma may cover the construction of the pluton. Indeed, Coleman et al. (2004) and Glazner et al. (2004) record the building of large plutons incrementally over ca 10 Myrs. On the other hand, the 613 Ma age may be tentatively attributed to the N–S directed sinistral event and to the coeval emplacement of the nearby BmG, because the structures of K104 have been reworked in the N–S direction. However, this event is only responsible for discrete solid-state deformation corridors in BHG and local crystallization of secondary minerals, hence it is unlikely to have induced the growth of new zircons. Whatever the case, we retain that 622 to 613 Ma is the age of building of Fomopéa pluton.

A high-K calk-alkaline granodiorite from Oban in southeastern Nigeria (close to the border with West Cameroon) was dated at 617 ± 1 Ma by Ekwueme and Kröner (1998). This granodiorite is very similar to the BHG unit of Fomopéa pluton, because it contains conspicuous porphyritic K-feldspar megacrysts, and hornblende and biotite as mafic minerals. The 613 Ma phase is also of importance in Cameroon, as it corresponds to the ages of magmatic rocks from the Lom area to the East (Toteu et al., 2006a). Opening of the Lom volcano-sedimentary basin may have occurred at that time, possibly along a N30 sinistral shear zone (Fig. 1). The Fomopéa pluton also shares petrological and geochronological affinities with the granitoids emplaced around and north of Ngaoundéré (Tchameni et al., 2006).

To the South, the feeding of the Yaoundé Group sediments has been recently pinned at ages younger than 625 Ma by the same authors. The southward thrusting of the Yaounde nappe over the Archaean Ntem craton is proposed to have occurred during the 600 to 570 Ma time interval (Toteu et al., 2006b; Moloto et al., 2008). Assuming that the Rocher du Loup shear zone (RLSZ) along the southwestern coast of Cameroon (Fig. 1) is a lateral ramp accommodating horizontal displacements due to the Yaoundé nappe by a sinistral wrench motion, the 590 Ma age of the synkinematic Rocher du Loup syenite would yield the age of the thrust tectonics in southern Cameroon (Toteu et al., 1994). Thus, emplacement of the Fomopéa pluton happened before this thrusting event. In this case, the local N–S reworking of the pluton may also be regarded as coeval with this sinistral movement along the RLSZ, and thus would be dated at 590 Ma. A possibly better correlation is offered by the sinistral N–S Mayo Nolti and Godé-Gormaya shear zones (respectively MNSZ and GGSZ in Fig. 1). Unfortunately, these two shear zones studied by Ngako et al. (2008) have not been dated so far. Therefore, the age of the D2 N–S sinistral event remains in debate at 613 or 590 Ma (Fig. 10).

The last Pan-African event in the area is the development of the dextral mylonitic shear zone to the southeast. The petrographic observations point to amphibolite facies conditions in the shear zone, associated to a strong lateral gradient, because the protomylonites at the southern border of the pluton only recorded greenschist facies conditions. The rest of the pluton does not seem to have been affected by these last deformation, with the noticeable exception of a perturbation of the Rb–Sr isotopic system, hence the 572 ± 48 Ma age obtained by Kwékam et al. (2009) using this method. Although imprecise, this age is consistent for the shear zone. Indeed, this shear zone belongs to the dextral Central Cameroon shear zone system, that can be regarded as the prolongation of the dextral Patos shear zone system in Brazil, dated at 576 ± 3 Ma by Archanjo et al. (2008).

8. Conclusion

The present study provides new results from the systematic study of magnetic fabrics and microstructures, that help to understand the links between the emplacement and deformation of the Fomopéa granitic pluton. Using the AMS data, magnetic properties and detailed petrographic observations, it has been possible (1) to determine pure multidomain magnetite as the mean magnetic susceptibility carrier, (2) to draw structural maps of the Fomopéa pluton, and (3) to reveal a polyphased Pan-African structural evolution deduced from the relative chronology of the plutonic fabrics. The geochronology of the different phases is derived from recent ages by Kwékam et al. (2009) in Fomopéa pluton and from former works elsewhere in Cameroon. Emplacement of the pluton likely occurred at 622 to 613 Ma, whereas the country rocks seem to record an earlier Pan-African phase. The pluton age is very similar to the ages of other high-K calk-alkaline intrusions in southeastern Nigeria as well as in northern Cameroon. In addition, emplacement of the BmG may have been coeval with a N–S striking sinistral deformation event, that was also responsible for localised N–S sinistral shear bands in BHG. This N–S sinistral transcurrent event may be correlated with other (undated) N–S shear zones of northwestern Cameroon, and possibly with another shear zone running along the southwestern coast, that has been dated at 590 Ma. Mylonitisation along the southeastern border of the pluton is the last Pan-African event in the study area. This NE–SW dextral shear zone is the prolongation of the Patos shear zone from Brazil in Cameroon, both of them being formed at ca 572 Ma. Therefore, the Fomopéa pluton registered about 50 Myrs of Pan-African deformation in West Cameroon.

Acknowledgements

The two first authors benefitted from a financial support of the AUF (Agence Universitaire de la Francophonie) through a research project no 6313PS566. In addition, T. Njanko received financial support from the IRD-CORUS project of M. Jessell and J.L. Bouchez from LMTG (Toulouse). Technical assistance by C. Cavaré-Hester, J.F. Ména and F. de Parseval is warmly acknowledged. IRD-Cameroon kindly provided a vehicle for field work in Fomopéa. Thoughtful reviews by P. Barbey and K. Benn contributed to improve the manuscript.

References

Anhaeusser, C.R., Mason, R., Viljoen, M.J., Viljoen, R.P., 1969. A reappraisal of some aspects of Precambrian shield geology. Geological Society of America Bulletin 80, 2175–2200.

Archanjo, C.J., Hollanda, M.H.B.M., Rodrigues, S.W.O., Neves, B.B.B., Armtrong, R., 2008. Fabrics of pre- and syntectonic granite plutons and chronology of shear zone in the Eastern Borborema province, NE Brazil. Journal of Structural Geology 30, 310–326.

Benn K. Anisotropy of magnetic susceptibility fabrics in syntectonic plutons as tectonic strain markers: example of the Canso pluton, Megume Tarrane, Nova Scotia. Earth and Environmental Transactions of the Royal Society of Edinburgh, in press.

Bouchez, J.L., 1997. Granite is never isotropic: an introduction to AMS studies of granitic rocks. In: Bouchez, J.L., Hutton, D.H.W., Stephens, W.E. (Eds.), Granite: From Segregation of Melt to Emplacement Fabrics. Kluwer Academic Publishers, Dordrecht, pp. 95–112.

Bouchez, J.L., 2000. Anisotropie de susceptibilité magnétique et fabrique des granites. Comptes Rendus Académie des Sciences, Paris, Earth and Planetary Sciences 330, 1–14.

Bouchez, J.-L., Delas, C., Gleizes, G., Nédélec, A., Cuney, M., 1992. Submagmatic microfractures in granites. Geology 20, 35–38.

Brown, M., Solar, G.S., 1998. Granite ascent and emplacement during contractional deformation in convergent orogens. Journal of Structural Geology 20, 1365–1393.

Brito Neves, B.B., Van Schmus, W.R., Fetter, A., 2002. North-western Africa-North-eastern Brazil: major tectonic links and correlation problems. Journal of African Earth Sciences 34, 275–278.

Caby, R., Sial, A.N., Arthaud, M., Vauchez, A., 1991. Crustal evolution and the Brasiliano orogeny in Northeast Brizil. In: Dallmeyer, R.D., Lécorché, J.C.P.L. (Eds.), The West African Orogens and Circum-Atlantic Correlatives. Springer-Verlag, Berlin, pp. 373–397.

Clemens, J.D., Petford, N., Mawer, C.K., 1997. Ascent mechanisms of granitic magmas: causes and consequences. In: Holness, M.B. (Ed.), Deformation-enhanced Fluid Transport in the Earth's Crust and Mantle. Chapman and Hall, London, pp. 144–171.

Coleman, D.S., Gray, W., Glazner, A.F., 2004. Rethinking the emplacement and evolution of zoned plutons: geochronological evidence for incremental assembly of the Tuolumne intrusive suite, California. Geology 32, 433–436.

Cordani, U.G., D'Agrella-Filho, M.S., Brito Neves, B.B., Trindade, R.I.F., 2003. Tearing up Rodinia: the Neoproterozoic palaeogeography of south American cratonic fragments. Terra Nova 15, 350–359.

D'Lemos, R.S., Brown, M., Strachan, R.A., 1992. Granite magma generation, ascent and emplacement within a transpressional orogen. Journal of the Geological Society, London 149, 487–490.

Day, R., Fuller, M.D., Schmidt, V.A., 1977. Interacting single-domain properties of magnetite intergrowth. Journal of Geophysical Research 81, 989–994.

Dumort, J.C., 1968. Carte géologique de reconnaissance à l'échelle 1/500 000 et notice explicative sur la feuille Douala-Ouest. Direction des mines et de la géologie du Cameroun.

Ekwueme, B.N., Kröner, A., 1998. Single zircon evaporation ages from the Oban Massif, southeastern Nigeria. Journal of African Earth Sciences 26, 195–205.

Gapais, D., 1989. Shear structures within deformed granites: mechanical and thermal indicators. Geology 17, 1144–1147.

Glazner, A.F., Barley, J.M., Coleman, D.S., Gray, W., Taylor, R.Z., 2004. Are plutons assembled over millions of years by amalgamation from small magma chambers? GSA Today 14, 4–11.

Grégoire, V., Darrozes, J., Gaillot, P., Nédélec, A., 1998. Magnetite grains shape fabric and distribution anisotropy vs. rock magnetic fabric: a three-dimensional case study. Journal of Structural Geology 20 (7), 937–944.

Hutton, D.W.H., 1997. Syntectonic granites and the principle of effective stress: a general solution to the space problem? In: Bouchez, J.L., Hutton, D.W.H., Stephens, W.E. (Eds.), Granite: from Segregation of Melt to Emplacement Fabrics. Kluwer Academic Publishers, Dordrecht, pp. 189–197.

Ingram, G.M., Hutton, D.W.H., 1994. The Great Tonalite sSill: emplacement into a contractional shear zone and implications for Late Cretaceous to early Eocene tectonics in southeastern Alaska and British Columbia. Geological Society of America Bulletin 106, 715–728.

Jelinek, V., 1978. Statistical processing of anisotropy of magnetic susceptibility measured on groups of specimens. Studia Geoph Geod 142, 50–62.

Jelinek, V., 1981. Characterization of the magnetic fabric of rocks. Tectonophysics 79, 563–567.

Kankeu, B., Greiling, O.R., 2006. Magnetic fabrics (AMS) and transpression in the Neoproterozoic basement of Eastern Cameroon (Garga-Sarali area). Neues Jahrbuch für Geologie und Paläontologie Abhandhungen 239, 263–287.

Kwékam, M., 2005. Genèse et évolution des granitoïdes calco-alcalins au cours de la tectonique Panafricaine: le cas des massifs syn- à tardi-tectoniques de l'Ouest –Cameroun (régions de Dschang et de Kekem). Thèse Doctorat d'Etat Université de Yaoundé I, 201 pp.

Kwékam, M., Liégeois, J.P., Njonfang, E., Affaton, P., Hartmann, G., Toteu, S.F., Tchoua, F., 2009. Nature, origin and significance of the Pan-African high-K calc-alkaline Fomopéa plutonic complex in the Central African fold belt (Cameroon). Journal of African Earth Sciences, in revision.

Lasserre, M., 1967a. Données géochronologiques nouvelles acquises au 1er janvier 1967 par la méthode au Strontium appliquée aux formations cristallines et cristallophylliennes du Cameroun. Annales dela Faculté des Sciences de l'Université de Clermont-Ferrand 36 (16), 109–144.

Lasserre, M., 1967b. Données nouvelles acquises, en géochronologie, par la méthode au Strontium appliquée à l'étude des massifs cristallins du Cameroun. Compte Rendu Sommaire de la Société géologique de France, fascicule 3, 89–90.

Leblanc, D., Gleizes, G., Roux, L., Bouchez, J.L., 1996. Variscan dextral transpression in the French Pyrenees: new data from the Pic des Trois-Seigneurs granodiorite and its country rocks. Tectonophysics 261, 331–345.

Liou, J.G., 1973. Synthesis and stability relations of epidote, $Ca_2Al_2FeSi_3O_{12}(OH)$. Journal of Petrology 14, 381–413.
Moloto-A-Kenguemba, G.R., Trindade, R.I.F., Monié, P., Nédélec, A., Siqueira, R., 2008. A late Neoproterozoic paleomagnetic pole for the Congo craton: Tectonic setting, paleomagnetism and geochronology of the Nola dike swarm (Central African Republic). Precambrian Research 164, 214–226.
Nascimento (do), H.S., Bouchez, J.L., Nédélec, A., Sabaté, P., 2004. Evidence of an early NS magmatic event in the Paleoproterozoic Teofilandia granitoids (São Francisco Craton, Brazil): a combined microstructural and magnetic fabric study. Precambrian Research 134, 41–59.
Ngako, V., Affaton, P., Nnange, J.M., Njanko, Th, 2003. Pan-African tectonic evolution in central and southern Cameroon: transpression and transtension during sinistral shear movements. Journal of African Earth Sciences 36, 207–214.
Ngako, V., Affaton, P., Njonfang, E., 2008. Pan-African tectonics in northwestern Cameroon: implication for the history of western Gondwana. Gondwana Research 14, 509–522.
Njanko, T., Nédélec, A., Affaton, P., 2006. Synkinematic high-K calc-alkaline plutons associated with the Pan-African Central Cameroon shear zone (W-Tibati area): petrology and geodynamic significance. Journal of African Earth Sciences 44 (4–5), 494–510.
Nzenti, J.P., Barbey, P., Macaudière, J., Soba, D., 1988. Origin and evolution of the late Precambrian high-grade Yaoundé gneisses (Cameroon). Precambrian Research 38, 91–109.
Paterson, S.R., Vernon, R.H., Tobisch, O.T., 1989. A review for the identification of magmatic and tectonic foliations in granitoids. Journal Structural Geology 11 (3), 349–363.
Penaye, J., Toteu, S.F., Michard, A., Bertrand, J.M., Dautel, D., 1989. Reliques granulitiques d'âge Proterozoïque inferieur dans la zone mobile Panafricaine d'Afrique Centrale au Cameroun; Geochronologie U-Pb sur zircons. Comptes Rendus de l'Académie des Sciences (Paris) 309, 315–318.
Penaye, J., Toteu, S.F., van Schmus, W.R., Nzenti, J.P., 1993. Données géochronologiques préliminaires (U–Pb et Sm–Nd) sur la série de Yaoundé: âge du métamorphisme granulitique de la zone mobile. Comptes Rendus de l'Académie des Sciences (Paris) 317, 789–797.
Pignotta, G.S., Benn, K., 1999. Magnetic fabrics of the Barrington passage pluton, Meguma Terrane, Nova Scotia: a two-stage fabric history of syntectonic emplacement. Tectonophysics 307, 75–92.
Razanatseheno, M.O.M., Nédélec, A., Rakotondrazafy, M., Ralison, B., Meert, J.G. Four-stage building of the Cambrian Carion pluton (Madagascar) revealed by AMS study. Earth and Environmental Transactions of the Royal Society of Edinburgh, 100, in press.
Rochette, P., 1987. Magnetic susceptibility of rock matrix related to magnetic fabric studies. Journal Structural Geology 9, 1015–1020.
Rochette, P., Jackson, M., Aubourg, C., 1992. Rock magnetism and the interpretation of anisotropy of magnetic susceptibility. Reviews of Geophysics 30, 209–222.
Sadeghian, M., Bouchez, J.L., Nédélec, A., Valizadeh, M.V., Siqueira, R., 2005. The granite pluton of Zahedan (SE-Iran): petrological and magnetic fabric study of a syntectonic sill emplaced in a transtensional setting. Journal of Asian Earth Sciences 25, 961–980.
Sial, A.N., Toselli, A.J., Saavedra, J., Parada, M.A., Ferreira, V.P., 1999. Emplacement, petrological and magnetic susceptibility characteristics of diverse magmatic epidote-bearing granitoid rocks in Brazil, Argentina and Chile. Lithos 46, 367–392.
Simpson, C., 1985. Deformation of granitic rocks across the brittle-ductile transition. Journal of Structural Geology 7, 503–511.
Solar, G.S., Pressley, R.A., Brown, M., Tucker, R.D., 1998. Granite ascent in convergent orogenic belts: testing a model. Geology 26, 711–714.
Tagné-Kamga, G., 2003. Petrogenesis of the Neoproterozoic Ngondo Plutonic complex (Cameroon, west central Africa): a case of late collisional ferro-potassic magmatism. Journal of African Earth Sciences 36, 149–171.
Tchameni, R., Pouclet, A., Penaye, J., Ganwa, A.A., Toteu, S.F., 2006. Petrography and geochemistry of the Ngaoundéré Pan-African granitoids in Central Cameroon: implications for their sources and geological setting. Journal of African Earth Sciences 44, 511–529.
Tetsopgang, S., Anami, M., Njonfang, E., 2006. Petrology of highly evolved Pan-African two-mica granites from the Nkambé area, West Cameroon. Journal of African Earth Sciences 46, 305–317.
Toteu, S.F., Van Schmus, W.R., Penaye, J., Nyobé, J.B., 1994. U–Pb and Sm–Nd evidence for Eburnean and Pan-African high-grade metamorphism in cratonic rocks of southern Cameroon. Precambrian Research 67, 321–347.
Toteu, S.F., Van Schmus, W.R., Penaye, J., Michard, A., 2001. New U–Pb and Sm–Nd data from north-central Cameroon and its bearing on the pre-Pan African history of central Africa. Precambrian Research 108, 45–73.
Toteu, S.F., Penaye, J., Deloule, E., Van Schmus, W.R., Tchameni, R., 2006a. Diachronous evolution of volcano-sedimentary basins north of the Congo craton: insights from U–Pb ion microprobe dating of zircons from the Poli, Lom and Yaounde Groups (Cameroon). Journal of African Earth Sciences 44, 428–442.
Toteu, S.F., Yongue Fouateu, R., Penaye, J., Tchakounte, J., Seme Mouangue, A.C., Van Schmus, W.R., Deloule, E., Stendal, H., 2006b. U–Pb dating of plutonic rocks involved in the nappe tectonic in southern Cameroon: consequence for the Pan-African orogenic evolution of the central African fold belt. Journal of African Earth Sciences 44, 479–493.